NANO LETTERS

pubs.acs.org/NanoLett Letter

Optical Quantification by Nanopores of Viruses, Extracellular Vesicles, and Nanoparticles

Léa Chazot-Franguiadakis, Joelle Eid, Marius Socol, Bastien Molcrette, Philippe Guégan, Marylène Mougel, Anna Salvetti, and Fabien Montel*

Cite This: https://doi.org/10.1021/acs.nanolett.2c00253 Read Online

ACCESS | Metrics & More | Article Recommendations | Supporting Information

ABSTRACT: Nanopores combined with optical approaches can be used to detect viral particles. In this work, we demonstrate the ability of hydrodynamical driving and optical sensing to identify and quantify viral particles in a biological sample. We have developed a simple and rapid method which requires only fluorescent labeling of the particles and can therefore be applied to a wide range of virus type. The system operates in real time and at the single particle level while providing a low error on concentration (4%) and a low limit of detection of 10^5 particles/mL for an acquisition time of 60 s with the ability to increase the acquisition time to achieve a lower limit.

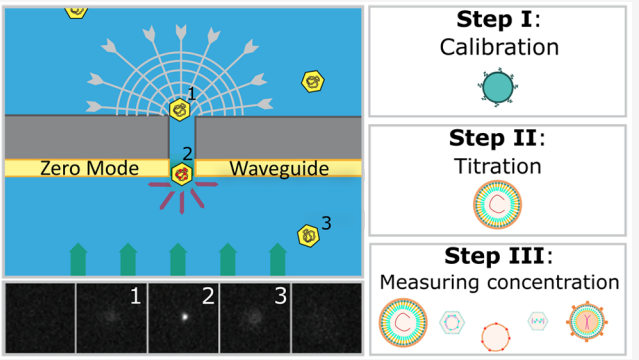

KEYWORDS: *Nanopore, Virus, Extracellular Vesicles, Nanoparticles, Zero Mode Waveguide, Concentration measurement*

INTRODUCTION

The rapid and accurate quantification of viruses is crucial to gain information on viral infection processes and is still a goal to achieve in clinical and basic research. Currently commercially available assays offer noteworthy detection limits, for example, 200 DNA copies/mL for quantitative commercial real-time polymerase chain reaction (qPCR)-based assays[1,2] or 6−10 × 10^5 particles/mL for Western Blot/ELISA assays.[3] In any case, these methods are time-consuming (about 24 h for ELISA or Western Blot), too specific (ELISA and Western Blot assays can be carried out only if a primary antibody against the protein of interest is available), and sometimes inaccurate (due to off-target effects and saturation of the signal).[4,5] Therefore, they do not fully respond to the requested specifications in several fields of application such as clinical diagnosis (live monitoring of virus levels in patient samples) and basic research which may focus on different stages of the virus cycle (entry into the cell, reverse transcription, release of new virions, and so forth). To meet demand, several microfluidic and single molecule-based quantification techniques are now under development.[5−7] For instance, commercial Nanoparticle Tracking Analysis (NTA) can be used to determine concentration and size distribution of fluorescent viral particles. NTA offers a limit of detection (LOD) of 10^6 particles/mL and a manipulation time of a few hours.[8−10] Interferometric light microscopy can also be used to quantify viruses while measuring scattered signal and Brownian motion but the LOD is elevated (10^8−10^{10} particles/mL).[11]

An interesting compromise between a low LOD and real-time acquisition can be found in nanopore devices that have been developed in recent years and have tended to become a new standard for DNA/RNA sequencing.[12,13] Nanopore devices with single-molecule and real-time detection capabilities are of great interest to detect and quantify viruses as they open new avenues for the development of simpler, faster, and more compact quantification alternatives. Most methods based on nanopores rely on genome detection and quantification with electrical sensing,[14−17] but optical detection is a possible alternative. In that sense, zero-mode waveguide (ZMW) methods combined with nanopores have been shown to be powerful tools as they allow enhanced DNA sequencing.[18−20]

Some other techniques using electrical detection, are probing the virus as a whole. These techniques, referred to as resistive pulse sensing techniques, are based on quantifying changes in resistance using a nanoscale constriction. In practice, a voltage is applied between the two sides of the pore, and when an object enters the pore the variations of the ionic current are measured.[21−23] It is thus possible to detect

Received: January 20, 2022
Revised: April 21, 2022

https://doi.org/10.1021/acs.nanolett.2c00253
Nano Lett. XXXX, XXX, XXX−XXX

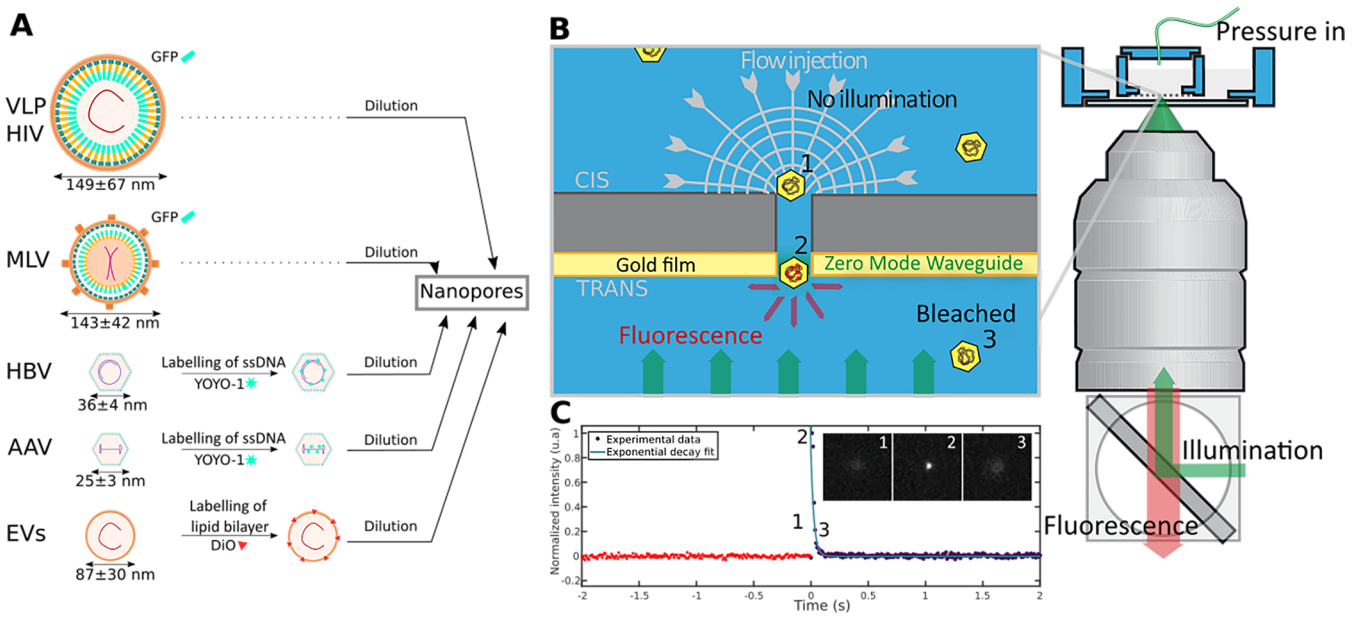

Figure 1. (A) Characteristics of particles and experimental protocol used in this study. From top to bottom: virus-like particle of human immunodeficience virus (VLP HIV); murine leukemia virus (MLV); Hepatitis B virus (HBV); adeno-associated virus (serotype 8 and 9) (AAV); extracellular vesicles (EVs). Fluorescent labeling of particles was required: it can be achieved by genome modification (GFP labeling for HIV and MLV) or directly by adding fluorophores in the sample (YOYO-1 for AAV and HBV, DiO for EVs). Potential cellular DNA is represented in red in VLP HIV and EVs, viral RNA in pink in MLV, and viral DNA in purple in HBV and AAV. Samples were then diluted. Sizes were determined by NTA for HIV, MLV, and EVs and by Cryo-EM reconstruction for AAV[37] and HBV.[38] (B) Zero mode waveguide setup for particles translocation through nanopores. The cis chamber contained the fluorescently labeled particles. Upon pressure application, the particles were pushed through the pore in the trans chamber and illuminated as soon as they cross the evanescent field region at the end of the pore. Once they have left the pore, they were unfocused and bleached. (C) Evolution of fluorescence of event as a function of time and snapshots of particle exit. Normalized intensity was represented as a function of time for AAV (violet and red points, averaged on N = 50 events). Normalized intensity was obtained by dividing intensity by the maximum intensity. Time was rescaled to zero at the beginning of an event and red points corresponded to intensity before the event. Exponential decay was represented in blue. Pore diameter 400 nm, Applied pressure 0.5 mbar. Frame rate: 112 fps. Inset: image size = 10 μm.

and quantify viruses with an interesting lower practical count limit of 5×10^7 particles/mL as reported by the De Blois and Wesley team.[24] Interestingly, these methods can be used to obtain information on the size of the objects and even establish size distribution profile,[25] because the variation in resistance of the pore is directly related to the sizes of the pore and of the object crossing it. Nevertheless, to date they mainly focus on the determination of particle size and not on a quantitative measurement of concentration.[26] This can be explained by some limitations of these systems, notably the fact that they remain too unspecific since any object passing through the pore will be detected, as well as objects that do not cross the pore but only come close to the surface and diffuse back. This represents a major bottleneck in order to quantify viral concentration. Moreover, it can be added that electrical detection can only detect particle transport in pores that are of the same diameter as the particle which increases plugging risk. This is not the case in optical detection where the pore can be much larger than the virus size.

Ultimately, despite these advances, a technological gap remains as there is no nanopore-optical technique to quantify virus concentration. It should be remembered that viruses are particular biological objects and whether for techniques using electrical or optical detection, the solid state nanopores are often made of SiN or SiC which makes the virus stick to the pore.

In this work, we proposed to use hydrodynamical driving of viral particles through artificial low cost nanopores and optical detection. We developed a simple and sensitive method which required only fluorescent labeling of particles and an initial calibration of our experimental setup. It allowed us to be more specific but also versatile. Moreover, the track-etched membranes that we used were particularly relevant for this type of application since they were optimized to reduce biofouling. We showed that our setup can be used to detect biological particles and accurately determine their concentration in a small volume of biological sample with a low LOD of about 10^5particles/mL for an acquisition time of 60 s (with the possibility to increase the acquisition time over 60 s to reach a lower LOD, for example, about 1 h to reach a LOD of 10^3 particles/mL). Moreover, we detected different types of viral particles and also discriminated viruses from extracellular vesicles to finally shed light on the versatility of the method.

RESULTS AND DISCUSSION

The viral particles used in this study are representative of the large range of virus population often encountered either for biotechnology application or as pathology generator: enveloped/nonenveloped, DNA, viruses, retroviruses as detailed in Figure 1A. As enveloped viruses, human immunodeficiency virus (HIV) was used as noninfectious virus-like particle (VLP) form. VLP structurally mimics the native virus but is devoid of the viral genome. It is a promising candidate for vaccination.[27] VLP HIV were obtained from monoclonal human HeLa cells stably expressing Gag-GFP. Murine leukemia virus (MLV) was used in the form of both VLP

https://doi.org/10.1021/acs.nanolett.2c00253
Nano Lett. XXXX, XXX, XXX−XXX

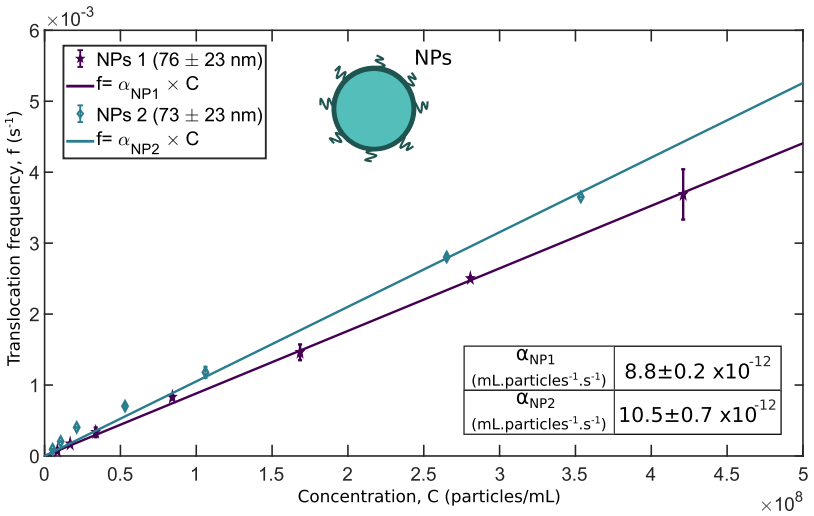

Figure 2. Calibration of the experimental setup using fluorescent polystyrene nanobeads (NPs). Translocation frequency (f), as a function of NPs concentration (C), for two batches of NPs. Continuous blue and violet curves corresponded to linear fit. Pore diameter 400 nm. Applied pressure 0.5 mbar. Experimental errors were the standard error of the mean and $N_{replica} > 36$ for each experimental series.

and complete enveloped virus cultivated from NIH3T3 mouse embryonic fibroblast cells. For these two retroviruses, fluorescent labeling relied on green fluorescent protein (GFP, λ_{exc} = 488 nm/λ_{em} = 507 nm) insertion into viral genome and expressed as Gag-GFP fusion,[28] which did not alter the properties of the virus.[29,30]

As nonenveloped viruses, we relied on adeno-associated virus (AAV, serotypes 8/9) which have gained interest for genetic therapies and vaccination processes over past years. Stocks of AAV-8 and AAV-9 recombinant particles were generated by calcium phosphate transfection of HEK-293 cells and analyzed by AFM as described previously in literature.[31,32] Hepatitis B Virus (HBV) was also used in a nonenveloped form (i.e., noninfectious form) that was purified from a viral stock of infectious HBV particles (genotype D) concentrated on a 20% sucrose cushion. AAV and HBV were fluorescently labeled using intercalating fluorophore YOYO-1 (Molecular Probes, 1 mM in DMSO, λ_{exc} = 491 nm/λ_{em} = 509 nm) which targets viral DNA.

Furthermore, we handled extracellular vesicles (EVs) which are constituted of lipids and proteins and sometimes contain cellular genetic material. Such compositions often lead them to be mistaken for viruses. EVs have been shown to play key roles in various cellular processes such as regulation and intercellular signaling but also in infectious diseases where they facilitate spreading, and escape from immune surveillance.[33−35] So far, few methods are able to distinguish viruses from EVs.[36] EVs used in this study were obtained from HIV- or MLV-producing cells and from uninfected cells. By using lipid bilayer markers DiO or DiL (Molecular Probes), we were able to fluorescently label EVs and to distinguish them from nonenveloped viruses. All particles were depicted in Figure 1A, and more precision can be found in Supporting Information.

Both particles with existing fluorescent label and without initial fluorescent label can be used. As for particles without initial fluorescent label, we used a one-step labeling procedure, which simply involved incubating the sample with a small volume of fluorophores (<1 μL) for a few minutes (10−15 min of incubation). By using several types of fluorophores, we were able to label a wide range of viruses as well as extracellular vesicles. Those fluorophores were passive markers without interaction with the nanopores, and therefore they did not alter the translocation of the viral particles (more information can be found in Supporting Information, S2). As mentioned, the particles were fluorescently labeled and then injected in the cis chamber of our setup. As shown in Figure 1B, a hydrodynamical driving induced by a pressure difference imposed by a microcontroller (MFCS, Fluigent) between the two sides of a nanoporous membrane (coated with a 50 nm thick gold layer on the trans side) was used to force translocation of particles from cis to trans side. The membranes used were track-etched membranes (Whatman, GE Polycarbonate) produced through heavy ion irradiation, and they are commercially available dense arrays of cylindrical nanopores of controlled diameter and high density (1×10^8 pores/cm^2). After crossing the membrane, successful translocation events were detected by a ZMW setup. Briefly, the nanoporous array was illuminated by a laser beam (λ_{exc} = 473 nm) on the trans side and the gold layer inhibited the propagation of light through the membrane. It also induced an enhancement of the electromagnetical field in the nanopore on a depth equivalent to the radius of the pore whereas the electrical field was null at the surface of the membrane.[39,40] This effect enabled to optically separate the fluorescence signal of translocating particles from particles in the bulk (see Supporting Information and ref 41). The main advantage of this method is its ability to detect events with a large parallelization (in our case 10^5 pores in parallel). All types of particles used in this study were successfully detected at the exit of nanopores with a signal-to-noise ratio superior to 2. An example of average fluorescence intensity pattern for AAV particle can be found in Figure 1C, as well as snapshots of particle exit. The fluorescence intensity was fitted by an exponential decay function and event durations were found to be 26 ± 4 ms for AAV, which allowed us to confirm that we were in a ZMW regime. Complementary experiences highlighting the benefits and relevance of the ZMW, as well as a simplistic ZMW translocation model, are available in Supporting Information, S2.

Thereafter, in order to be able to determine virus concentration with our ZMW setup, we first made a calibration of nanoporous membranes using fluorescent carboxyl polystyrene nanobeads (NPs, Spherotech Inc.) from two batches

https://doi.org/10.1021/acs.nanolett.2c00253
Nano Lett. XXXX, XXX, XXX−XXX

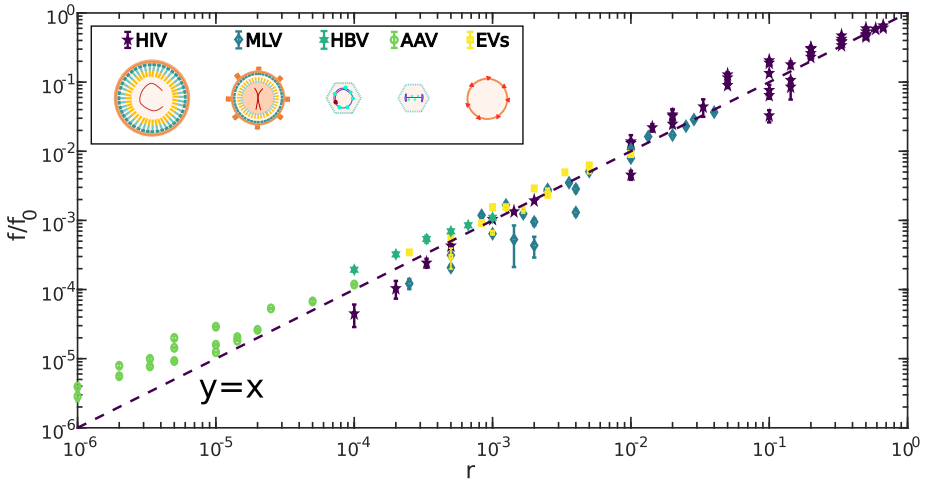

Figure 3. Effect of dilution factor on frequencies of translocation for all biological samples used in this study. Translocation frequency (f) normalized by initial translocation frequency (f_0) as a function of dilution factor (r). For each particle type, different diluted solutions were made from the same initial sample. Pore diameter 400 nm, Applied pressure 0.5 mbar. Experimental errors were the standard error of the mean, and $N_{replica} > 24$ for each experimental series.

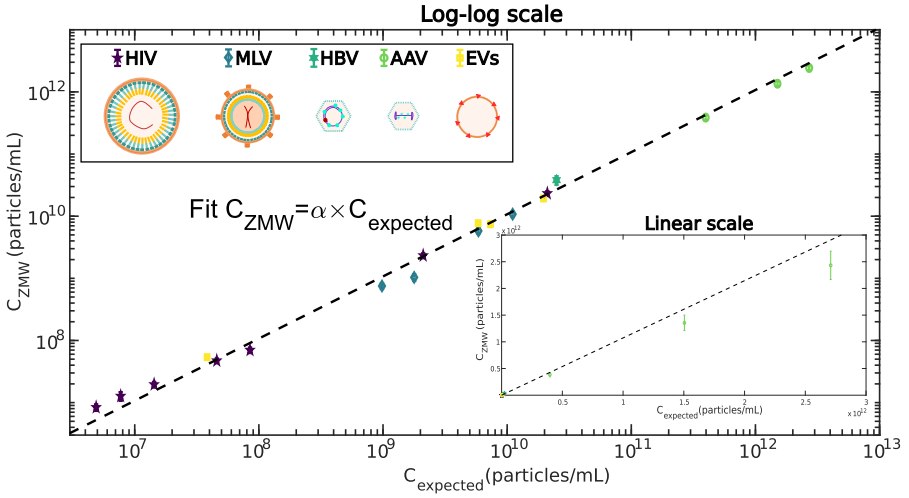

Figure 4. Comparison between concentrations obtained with our experimental setup (C_{ZMW}) and expected concentrations ($C_{expected}$) obtained with other methods (qPCR and NTA). Each point corresponded to a different sample. Results were depicted in log−log scale and also linear scale in the inset. Error bars took into account standard error for f_0 and the error on the calibration coefficient α_{NP}.

(with sizes determined by DLS measurement) and of known concentrations. Nanobeads were smaller than pore size and acted as flow markers. Indeed, we assumed that the system was dominated by advection (Peclet number, $P_e > 1$, see Supporting Information) and that the flow in our system verified the Hagen−Poiseuille law.[42] This was supported by the fact that we observed a linear increase of translocation frequency of nanobeads with pressure (see Supporting Information).

To perform calibration, we analyzed the variation of the nanobeads' translocation frequency per pore, f, as a function of the concentration, C. The data for both types of nanobeads through pores of 400 nm and at applied pressure of 0.5 mbar were plotted on Figure 2. The mean of the experimental slope for both types of NPs, α_{NP} ($9.7 \times 10^{-12} \pm 0.7 \times 10^{-12}$ mL·particles^{-1}·s^{-1}) was calculated and gave a direct relation between translocation frequency and concentration. We then compared α_{NP} with a coefficient obtained theoretically to validate our calibration (see Supporting Information, S4).

On the basis of this calibration, we were then able to determine the viral particles concentration in biological samples. To do so, we measured the translocation frequency for a series of dilutions originating from the same sample. The particle translocation frequency (f) normalized by the particle translocation frequency for the initial sample (f_0) was represented as a function of the dilution ratio (r) on Figure 3. f_0 was obtained by linear extrapolation from particle translocation frequency (f) when $r = 1$. Each point corresponded to an experiment carried out with a single diluted sample and for each viral type. For each particle type, there were at least four different initial samples of unknown concentration. The linearity of the curve threw light on the fact that each particle going through a nanopore was effectively detected and no jamming effect occurred in the pore.

Initial concentration can then be obtained using calibration coefficient α_{NP} and the translocation frequency for the initial sample (f_0) relying on the following formula

https://doi.org/10.1021/acs.nanolett.2c00253
Nano Lett. XXXX, XXX, XXX−XXX

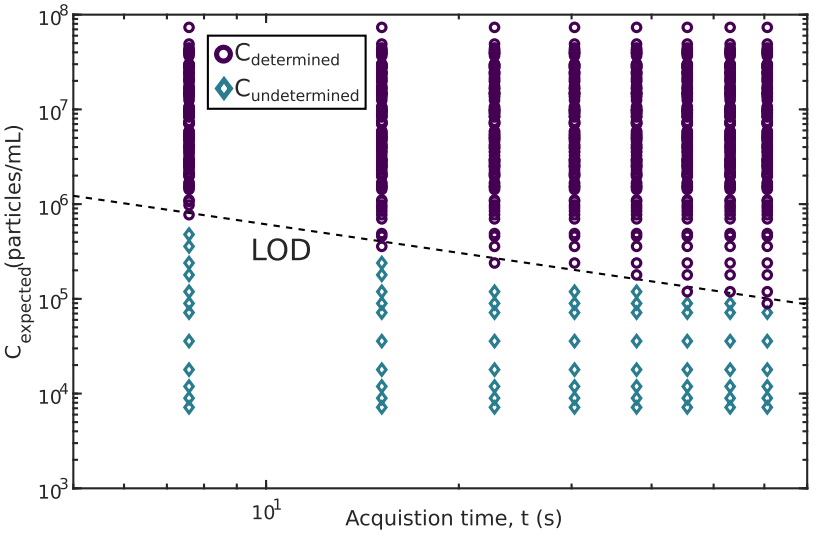

Figure 5. Expected concentrations (C) as a function of acquisition time (t). The black dashed line corresponds to the theoretical LOD. The violet circle represents the concentrations that could have been determined using our setup while the blue diamonds show the concentrations that could not have been measured (no event of translocation detected). Each point corresponds to a diluted sample originating from a viral particle sample whose concentration was determined previously.

$$C_{\mathrm{ZMW}} = \frac{f_0}{\alpha_{\mathrm{NP}}} \tag{1}$$

We compared the initial concentrations obtained for each biological sample to expected concentrations that had been obtained by qPCR (for AAV and HBV samples) and NTA (for HIV, MLV, and EVs samples). Results were presented in Figure 4. We observed a good agreement between measured values using ZMW setup and expected values over six decades of concentrations. The slope of the linear fit was equal to 0.96, which stood for 4% of error on our measurement. These results threw light on the versatility of our system, since we obtained a good precision for the concentration of all types of particles that were tested. It has to be recalled that each analysis was performed for 60 s, providing a total analysis duration of less than 15 min. Indeed, the total experimental duration included the incubation time required for the fluorescent labeling of the particles. However, incubation time can be performed at the beginning of an experiment set (for several samples) which allowed time to be saved.

Finally, given the large range of examined concentrations we were then interested in determining the limit of detection of our system. To do so, we first determined the LOD theoretically by suggesting that it was reached when a single event was detected in our sytem, at given experimental conditions. As mentioned earlier, we assumed that the Hagen–Poiseuille law was valid. In this case, the flow through a single pore J, at applied pressure ΔP, can be expressed as follows: $J = \frac{\Delta P}{R_{\mathrm{h}}}$ with $R_{\mathrm{h}} = \frac{8\eta L}{\pi R^4}$, R and L are the radius and the length of the pore, respectively, and η is the water viscosity.

Therefore, the total number of particles, N_{tot}, at a given concentration C, going through the area of the observed surface S, during an acquisition time t, came as $N_{\mathrm{tot}} = \frac{\Delta P \cdot N_{\mathrm{A}} \cdot t \cdot \sigma \cdot S}{R_{\mathrm{h}}} \cdot C$where σ is the pore density and N_{A} is the Avogadro number.

This led to the following formula for the limit of detection (LOD), which was defined as the concentration when the number of observed particles was equal to 1

$$\mathrm{LOD} = \frac{R_{\mathrm{h}}}{\Delta P \cdot N_{\mathrm{A}} \cdot t \cdot \sigma \cdot S} \tag{2}$$

The LOD was then tested experimentally as shown on Figure 5 on low concentration samples. We plotted the expected concentrations of different viral samples (HIV and AAV), C, as a function of the acquisition time, t. In order to prepare virus solutions at a given low concentration, a range of dilution was performed on a previously measured sample. The black dashed line corresponded to the theoretical LOD. Above this value, the violet circles represented the concentrations that could have been determined using our setup while the blue diamonds were the concentrations that could not be measured (no event detected). Almost all of the determined concentrations were above the theoretical LOD. Therefore, it represented a good estimation of the limit of our system. We concluded that the LOD of our system was about 10^5 particles/mL for an acquisition time of 60 s. Nevertheless, it was also possible to increase the acquisition time over 60 s to reach a lower LOD (for example, about 1 h to reach a LOD of 10^3 particles/mL).

Last but not least, since there is an ongoing need for direct counting of biotic nanoparticles such as viruses to probe the state of river water, we performed experiments on water coming from a river. Water was collected in the Rhône at Lyon (France, 4543′34.497″ North, 449′14.402″ East) on September 1, 2021. We first filtered the sample through 0.45 μm pores. We then divided our sample into two parts and fluorescently labeled one of them with YOYO-1 and the other one with DiO. The concentrations obtained using the ZMW setup were 2×10^7 particles/mL for the YOYO-1 labeled sample and 4×10^7 particles/mL for the DiO labeled sample (more information can be found in Supporting Information, S3). Labeling with YOYO-1 allowed us to detect and quantify viruses without envelope such as phytoplankton double-stranded DNA viruses (myovirus, podovirus, siphovirus)[11] or even adenovirus and norovirus that can be found in river water.[43] While labeling with DiO allowed us to detect and quantify both viruses with envelope (such as herpesvirus, HIV,

https://doi.org/10.1021/acs.nanolett.2c00253
Nano Lett. XXXX, XXX, XXX−XXX

and coronavirus including SARS-Cov-2)[44−46] and extracellular vesicles.[11] The concentrations that were found with our method agreed with the values given in literature for other rivers such as the Marne (in Paris France).[11]

CONCLUSION

All together these results showed that a combination of a near-field optics technique and fluorescence provided a powerful tool to detect the translocation of an individual virus through solid-state nanopores and to quantify their concentration.

Compared to other available methods, the main advantages of our strategy are that we achieved a low LOD and required a small volume of sample while keeping a short experimental duration and a specificity level that can be tuned by the final user. A comparison of the specifications and limits for different quantification methods can be found in Supporting Information (S4).

More precisely, our technique allowed one to work in real time at the scale of the single particle and to consider the virus as a whole compared to other methods which quantify DNA or specific proteins. The system offered a good precision (4% of error on the concentration) and a low LOD which was adjustable according to the experimental parameters. Moreover, it was possible to quantify the viral particles directly from complex biological samples (cell medium) comparable to clinical samples but also from real world samples (for example river water) while requiring small volumes. For viral samples whose concentrations were closed to the LOD (10^5 particles/mL), the required volume dropped down to 20 μL. It must be added that for highly concentrated samples, a dilution step was required to ensure that the linear regime is observed. This can be easily achieved by making a range of dilutions from the same initial sample and by checking that the translocation frequency evolved linearly with the concentration. Working in a diluted regime was valuable to avoid interactions between viruses. We have added a complementary experiment in Supporting Information (S3) to provide additional information about the necessity of working in a diluted mode.

Moreover, a major benefit of our system was its versatility since the fluorescent labeling can be adapted to a large range of virus type. By choosing specific fluorophores of different emission lengths, it was also possible to detect a mixture of viruses in the same sample by matching the fluorescent tags to the sought viruses. Therefore, two viruses labeled with a different fluorophore could be distinguished. Besides, the use of specific fluorescent labels prevented us from having signals coming from nontarget particles.

This system also had the advantage of using low cost solid-state nanopores, because the nanoporous membranes used were track-etched polycarbonate membranes used for water filtration that allowed one to detect events with a large parallelization (10^5 pores in parallel).

Last but not least, a miniaturization of our system can definitely be considered in the near future. The scope of applications of such a system could be great in basic research but also in clinic for titration purposes.

ASSOCIATED CONTENT

Supporting Information

The Supporting Information is available free of charge at https://pubs.acs.org/doi/10.1021/acs.nanolett.2c00253.

(S1) material and methods (viral particles production, quantification methods, calibration of experimental setup, zero mode waveguide setup, image analysis); (S2) fluorescence labeling (fluorescence tests on YOYO-1, fluorescence enhancement and ZMW); (S3) concentration regime and real world sample (concentration regime, river sample), (S4) comparison of calibration with theory; (S5) comparison with other existing techniques (PDF)

AUTHOR INFORMATION

Corresponding Author

Fabien Montel − *Laboratoire de Physique, UMR CNRS 5672, ENS de Lyon, Université de Lyon, Lyon 69007, France;* orcid.org/0000-0001-5430-864X; Email: fabien.montel@ens-lyon.fr

Authors

Léa Chazot-Franguiadakis − *Laboratoire de Physique, UMR CNRS 5672, ENS de Lyon, Université de Lyon, Lyon 69007, France*

Joelle Eid − *Institut de Recherche en Infectiologie de Montpellier, UMR CNRS 9004, Université de Montpellier, Montpellier 34965, France*

Marius Socol − *Institut de Recherche en Infectiologie de Montpellier, UMR CNRS 9004, Université de Montpellier, Montpellier 34965, France*

Bastien Molcrette − *Laboratoire de Physique, UMR CNRS 5672, ENS de Lyon, Université de Lyon, Lyon 69007, France*

Philippe Guégan − *Institut Parisien de Chimie Moléculaire, UMR CNRS 8232, Sorbonne Université, Paris 75252, France;* orcid.org/0000-0002-4919-0779

Marylène Mougel − *Institut de Recherche en Infectiologie de Montpellier, UMR CNRS 9004, Université de Montpellier, Montpellier 34965, France;* orcid.org/0000-0002-0345-1427

Anna Salvetti − *Centre International de Recherche en Infectiologie, UMR CNRS 5308, Université de Lyon, INSERM, Lyon 69007, France*

Complete contact information is available at: https://pubs.acs.org/10.1021/acs.nanolett.2c00253

Notes

The authors declare no competing financial interest.

ACKNOWLEDGMENTS

The authors thank Cendrine Moskalenko and Martin Castelnovo for their fruitful comments and discussions. This work was supported by the Centre National de la Recherche Scientifique under the 80 Prime project "NanoViro".

REFERENCES

(1) De Pagter, P. J.; Schuurman, R.; De Vos, N. M.; Mackay, W.; Van Loon, A. M. Multicenter external quality assessment of molecular methods for detection of human herpesvirus 6. *Journal of Clinical Microbiology* **2010**, *48*, 2536−2540.

(2) Ruiz-Villalba, A.; Ruijter, J. M.; van den Hoff, M. J. Use and misuse of cq in qpcr data analysis and reporting. *Life* **2021**, *11*, 496.

(3) Coorssen, J. R.; Blank, P. S.; Albertorio, F.; Bezrukov, L.; Kolosova, I.; Backlund, P. S.; Zimmerberg, J. Quantitative femto- to attomole immunodetection of regulated secretory vesicle proteins critical to exocytosis. *Anal. Biochem.* **2002**, *307*, 54−62.

(4) Ghosh, R.; Gilda, J. E.; Gomes, A. V. Accuracy of Western Blots. *Expert Review of Proteomics* **2014**, *11*, 549−560.
(5) Eid, J.; Mougel, M.; Socol, M. Advances in Continuous Microfluidics-Based Technologies for the Study of HIV Infection. *Viruses* **2020**, *12*, 982.
(6) Renner, T. M.; Tang, V. A.; Burger, D.; Langlois, M.-A. Intact Viral Particle Counts Measured by Flow Virometry Provide Insight into the Infectivity and Genome Packaging Efficiency of Moloney Murine Leukemia Virus. *Journal of Virology* **2020**, *94*, 1−17.
(7) Welsh, J. A.; van der Pol, E.; Bettin, B. A.; Carter, D. R.; Hendrix, A.; Lenassi, M.; Langlois, M. A.; Llorente, A.; van de Nes, A. S.; Nieuwland, R.; Tang, V.; Wang, L.; Witwer, K. W.; Jones, J. C. Towards defining reference materials for measuring extracellular vesicle refractive index, epitope abundance, size and concentration. *Journal of Extracellular Vesicles* **2020**, *9*, 1816641.
(8) Kramberger, P.; Ciringer, M.; Štrancar, A.; Peterka, M. Evaluation of nanoparticle tracking analysis for total virus particle determination. *Virology Journal 2012 9:1* **2012**, *9*, 1−10.
(9) Nikitin, N.; Trifonova, E.; Evtushenko, E.; Kirpichnikov, M.; Atabekov, J.; Karpova, O. Comparative Study of Non-Enveloped Icosahedral Viruses Size. *PLoS One* **2015**, *10*, e0142415.
(10) Steppert, P.; Burgstaller, D.; Klausberger, M.; Tover, A.; Berger, E.; Jungbauer, A. Quantification and characterization of virus-like particles by size-exclusion chromatography and nanoparticle tracking analysis. *Journal of Chromatography A* **2017**, *1487*, 89−99.
(11) Roose-Amsaleg, C.; Fedala, Y.; Vénien-Bryan, C.; Garnier, J.; Boccara, A. C.; Boccara, M. Utilization of interferometric light microscopy for the rapid analysis of virus abundance in a river. *Research in Microbiology* **2017**, *168*, 413−418.
(12) Workman, R. E.; et al. Nanopore native RNA sequencing of a human poly(A) transcriptome. *Nature Methods 2019 16:12* **2019**, *16*, 1297−1305.
(13) De Coster, W.; Weissensteiner, M. H.; Sedlazeck, F. J. Towards population-scale long-read sequencing. *Nat. Rev. Genet.* **2021**, *22*, 572−587.
(14) McNaughton, A. L.; Roberts, H. E.; Bonsall, D.; de Cesare, M.; Mokaya, J.; Lumley, S. F.; Golubchik, T.; Piazza, P.; Martin, J. B.; de Lara, C.; Brown, A.; Ansari, M. A.; Bowden, R.; Barnes, E.; Matthews, P. C. Illumina and Nanopore methods for whole genome sequencing of hepatitis B virus (HBV). *Sci. Rep.* **2019**, *9*, 1−14.
(15) Radukic, M. T.; Brandt, D.; Haak, M.; Müller, K. M.; Kalinowski, J. Nanopore sequencing of native adeno-associated virus (AAV) single-stranded DNA using a transposase-based rapid protocol. *NAR Genomics and Bioinformatics* **2020**, *2*, 1−16.
(16) Nguyen Quang, N.; Goudey, S.; Ségéral, E.; Mohammad, A.; Lemoine, S.; Blugeon, C.; Versapuech, M.; Paillart, J. C.; Berlioz-Torrent, C.; Emiliani, S.; Gallois-Montbrun, S. Dynamic nanopore long-read sequencing analysis of HIV-1 splicing events during the early steps of infection. *Retrovirology* **2020**, *17*, 1−24.
(17) Stein, U.; Meller, A.; Rozevsky, Y.; Gilboa, T.; Van Kooten, X. F.; Kobelt, D.; Huttner, D. Quantification of mRNA expression using single-molecule nanopore sensing. *ACS Nano* **2020**, *14*, 13964−13974.
(18) Farhangdoust, F.; Cheng, F.; Liang, W.; Liu, Y.; Wanunu, M. Rapid Identification of DNA Fragments through Direct Sequencing with Electro-Optical Zero-Mode Waveguides. *Adv. Mater.* **2022**, *34*, 2108479.
(19) Spitzberg, J. D.; Zrehen, A.; van Kooten, X. F.; Meller, A. Plasmonic-Nanopore Biosensors for Superior Single-Molecule Detection. *Adv. Mater.* **2019**, *31*, 1900422.
(20) Klughammer, N.; Dekker, C. Palladium zero-mode waveguides for optical single-molecule detection with nanopores. *Nanotechnology* **2021**, *32*, 18LT01.
(21) Harms, Z. D.; Haywood, D. G.; Kneller, A. R.; Selzer, L.; Zlotnick, A.; Jacobson, S. C. Single-particle electrophoresis in nanochannels. *Anal. Chem.* **2015**, *87*, 699−705.
(22) Harms, Z. D.; Selzer, L.; Zlotnick, A.; Jacobson, S. C. Monitoring Assembly of Virus Capsids with Nanofluidic Devices. *ACS Nano* **2015**, *9*, 9087−9096.
(23) McMullen, A.; De Haan, H. W.; Tang, J. X.; Stein, D. Stiff filamentous virus translocations through solid-state nanopores. *Nat. Commun.* **2014**, *5*, 1−10.
(24) DeBlois, R. W.; Wesley, R. K. Sizes and concentrations of several type C oncornaviruses and bacteriophage T2 by the resistive-pulse technique. *Journal of Virology* **1977**, *23*, 227−233.
(25) Vogel, R.; Willmott, G.; Kozak, D.; Roberts, G. S.; Anderson, W.; Groenewegen, L.; Glossop, B.; Barnett, A.; Turner, A.; Trau, M. Quantitative Sizing of Nano/Microparticles with a Tunable Elastomeric Pore Sensor. *Anal. Chem.* **2011**, *83*, 3499−3506.
(26) Yang, L.; Yamamoto, T. Quantification of virus particles using nanopore-based resistive-pulse sensing techniques. *Frontiers in Microbiology* **2016**, *7*, 1−7.
(27) Cervera, L.; Gòdia, F.; Tarrés-Freixas, F.; Aguilar-Gurrieri, C.; Carrillo, J.; Blanco, J.; Gutiérrez-Granados, S. Production of HIV-1-based virus-like particles for vaccination: achievements and limits. *Appl. Microbiol. Biotechnol.* **2019**, *103*, 7367−7384.
(28) Jouvenet, N.; Neil, S. J. D.; Zhadina, M.; Zang, T.; Kratovac, Z.; Lee, Y.; McNatt, M.; Hatziioannou, T.; Bieniasz, P. D. Broad-Spectrum Inhibition of Retroviral and Filoviral Particle Release by Tetherin. *Journal of Virology* **2009**, *83*, 1837−1844.
(29) Voelkel, C.; Galla, M.; Maetzig, T.; Warlich, E.; Kuehle, J.; Zychlinski, D.; Bode, J.; Cantz, T.; Schambach, A.; Baum, C. Protein transduction from retroviral Gag precursors. *Proc. Natl. Acad. Sci. U. S. A.* **2010**, *107*, 7805−7810.
(30) Mougel, M.; Akkawi, C.; Chamontin, C.; Feuillard, J.; Pessel-Vivares, L.; Socol, M.; Laine, S. NXF1 and CRM1 nuclear export pathways orchestrate nuclear export, translation and packaging of murine leukaemia retrovirus unspliced RNA. *RNA Biology* **2020**, *17*, 528−538.
(31) Salvetti, A.; Oreve, S.; Chadeuf, G.; Favre, D.; Cherel, Y.; Champion-Arnaud, P.; David-Ameline, J.; Moullier, P. Factors influencing recombinant adeno-associated virus production. *Hum. Gene Ther.* **1998**, *9*, 695−706.
(32) Carrasco-Salas, Y.; Malapert, A.; Sulthana, S.; Molcrette, B.; Chazot-Franguiadakis, L.; Bernard, P.; Chédin, F.; Faivre-Moskalenko, C.; Vanoosthuyse, V. The extruded non-template strand determines the architecture of R-loops. *Nucleic acids research* **2019**, *47*, 6783−6795.
(33) Paolini, L.; Zendrini, A.; Radeghieri, A. Biophysical properties of extracellular vesicles in diagnostics. *Biomarkers in Medicine* **2018**, *12*, 383−391.
(34) Giannessi, F.; Aiello, A.; Franchi, F.; Percario, Z. A.; Affabris, E. The role of extracellular vesicles as allies of HIV, HCV and SARS viruses. *Viruses* **2020**, *12*, 571.
(35) LeClaire, M.; Gimzewski, J.; Sharma, S. A review of the biomechanical properties of single extracellular vesicles. *Nano Select* **2021**, *2*, 1−15.
(36) Hoen, E. N.; Cremer, T.; Gallo, R. C.; Margolis, L. B. Extracellular vesicles and viruses: Are they close relatives? *Proc. Natl. Acad. Sci. U.S.A.* **2016**, *113*, 9155−9161.
(37) DiMattia, M. A.; et al. Structural Insight into the Unique Properties of Adeno-Associated Virus Serotype 9. *Journal of Virology* **2012**, *86*, 6947−6958.
(38) Crowther, R. A.; Kiselev, N. A.; Böttcher, B.; Berriman, J. A.; Borisova, G. P.; Ose, V.; Pumpens, P. Three-dimensional structure of hepatitis B virus core particles determined by electron cryomicroscopy. *Cell* **1994**, *77*, 943−950.
(39) Levene, H. J.; Korlach, J.; Turner, S. W.; Foquet, M.; Craighead, H. G.; Webb, W. W. Zero-mode waveguides for single-molecule analysis at high concentrations. *Science* **2003**, *299*, 682−686.
(40) Zhu, P.; Craighead, H. G. Zero-mode waveguides for single-molecule analysis. *Annual Review of Biophysics* **2012**, *41*, 269−293.
(41) Auger, T.; Mathé, J.; Viasnoff, V.; Charron, G.; Di Meglio, J. M.; Auvray, L.; Montel, F. Zero-mode waveguide detection of flow-driven DNA translocation through nanopores. *Phys. Rev. Lett.* **2014**, *113*, 1−5.

https://doi.org/10.1021/acs.nanolett.2c00253
Nano Lett. XXXX, XXX, XXX−XXX

(42) Kavokine, N.; Netz, R. R.; Bocquet, L. Fluids at the Nanoscale: From Continuum to Subcontinuum Transport. *Annu. Rev. Fluid Mech.* **2021**, *53*, 377−410.
(43) Sedji, M. I.; Varbanov, M.; Meo, M.; Colin, M.; Mathieu, L.; Bertrand, I. Quantification of human adenovirus and norovirus in river water in the north-east of France. *Environmental Science and Pollution Research* **2018**, *25*, 30497−30507.
(44) Ye, Y.; Ellenberg, R. M.; Graham, K. E.; Wigginton, K. R. Survivability, Partitioning, and Recovery of Enveloped Viruses in Untreated Municipal Wastewater. *Environ. Sci. Technol.* **2016**, *50*, 5077−5085.
(45) Bibby, K.; Peccia, J. Identification of viral pathogen diversity in sewage sludge by metagenome analysis. *Environ. Sci. Technol.* **2013**, *47*, 1945−1951.
(46) Guerrero-Latorre, L.; Ballesteros, I.; Villacrés-Granda, I.; Granda, M. G.; Freire-Paspuel, B.; Ríos-Touma, B. SARS-CoV-2 in river water: Implications in low sanitation countries. *Sci. Total Environ.* **2020**, *743*, 140832.

https://doi.org/10.1021/acs.nanolett.2c00253
Nano Lett. XXXX, XXX, XXX−XXX